Journal of Alloys and Compounds 577 (2013) 650–657

Contents lists available at SciVerse ScienceDirect

Journal of Alloys and Compounds

journal homepage: www.elsevier.com/locate/jalcom

Nanoquasicrystalline Al–Fe–Cr–Nb alloys produced by powder metallurgy

F. Audebert [a,b,*], M. Galano [b], C. Triveño Rios [c], H. Kasama [c], M. Peres [c], C. Kiminami [c], W.J. Botta [c], C. Bolfarini [c]

[a] Advanced Materials Group, Facultad de Ingeniería, Universidad de Buenos Aires. Paseo Colón 850, Buenos Aires 1063, Argentina
[b] Department of Materials, University of Oxford, Parks Road, OX1 3PH Oxford, UK
[c] Departamento de Engenharia de Materiais, Universidade Federal de São Carlos. Rodovia Washington Luiz, km 235, 13.565-905, PO Box 676, São Carlos, SP, Brazil

ARTICLE INFO

Article history:
Received 26 April 2013
Received in revised form 26 June 2013
Accepted 27 June 2013
Available online 5 July 2013

Keywords:
Aluminium alloys
Quasicrystals
Rapid solidification
Powder metallurgy

ABSTRACT

Nano-quasicrystalline Al–Fe–Cr based alloys produced by rapid solidification processes exhibit high strength at elevated temperatures. Nevertheless, the quasicrystalline particles in these systems become unstable at high temperature limiting the industrial applications. In early works, it was observed that the use of Nb or Ta increases the stability of the Al–Fe–Cr quasicrystalline phase delaying the microstructural transformation to higher temperatures. Thus, these nano-quasicrystalline Al-based alloys have become promising new high strength material to be used at elevated temperatures in the automotive and aeronautical industries. In previous works, nano-quasicrystalline Al–Fe–Cr–Nb based alloys were obtained by rapid solidification using the melt-spinning technique. In order to obtain bulk alloys for industrial applications other fabrication routes such as powder production by gas atomization followed by compaction and extrusion are required. In the present work, the production of Al–Fe–Cr–Nb based alloys by powder atomization at laboratory scale was investigated. The powders obtained were sieved in different ranges of sizes and the microstructures were characterised by means of X-ray diffraction, scanning and transmission electron microscopy, and energy dispersive of X-ray analysis. Mechanical properties have been measured by compression tests at room temperature and at 250 °C. It was observed that a very high temperature is required to produce these alloys by gas atomization; the icosahedral quasicrystalline phase can be retained after the atomization in powder sizes typically under 75 μm, and also after the extrusion at 375 °C. The extruded bars were able to retain a very high strength at elevated temperature, around 60% of the yield stress at room temperature, in contrast with the 10–30% typically obtained for many commercial Al alloys.

© 2013 Elsevier B.V. All rights reserved.

1. Introduction

Rapid solidification (RS) processes lead to obtain stable and/or metastable phases with a nano-scale size and higher solute content retained in the solid solution compared to the common casting processes [1]. RS processes allow producing nano-structured Al-based alloys which exhibit high strength in comparison with the current commercial Aluminium alloys [2]. Among the different nano-structured Al alloys reported in particular the nano-quasicrystalline Al–Fe–Cr based alloys produced by melt-spinning, composed of nano-quasicrystalline particles embedded in an fcc-Al matrix showed the best combination of high strength and acceptable plasticity at elevated temperatures [3]. However, the quasicrystalline particles in these systems become unstable at high temperature limiting the industrial applications [3]. In early works, it was observed that the addition of Ti, V, Nb or Ta improved the icosahedral quasicrystalline phase formation [4,5]. Particularly, Nb and Ta also increased the stability of the quasicrystalline phase delaying its microstructural transformation to higher temperatures [4–6]. Thus, nano-quasicrystalline Al–Fe–Cr–(Nb or Ta) alloys have become very promising new high strength light weight alloys to be applied at elevated temperatures in the automotive, aeronautical and aerospace industries.

In order to obtain these alloys in bulk shape for industrial applications powder production by gas atomization followed by compaction and extrusion is one of the promising technologies that would be used to obtain these high strength Al alloys in an industrial scale. Gas atomization has different characteristics than the melt-spinning technique used at laboratory scale which makes it crucial to study the feasibility to retain the complex Al–Fe–Cr–Nb nano-quasicrystalline particles in the gas atomized powders.

* Corresponding author at: Advanced Materials Group, Facultad de Ingeniería, Universidad de Buenos Aires, Paseo Colón 850, Buenos Aires 1063, Argentina.
E-mail addresses: metal@fi.uba.ar, fernando.audebert@materials.ox.ac.uk (F. Audebert).

0925-8388/$ - see front matter © 2013 Elsevier B.V. All rights reserved.
http://dx.doi.org/10.1016/j.jallcom.2013.06.162

Table 1
Alloys denomination, nominal chemical composition and thermal conditions of the gas atomization process.

Alloy denomination	Nominal composition (at%)	Molten alloy temperature (°C)	Holding time at Molten state (min)	Casting temperature (°C)
Nb(1)	$Al_{93}Fe_3Cr_2Nb_2$	1250	90	1250
Nb(2)	$Al_{93}Fe_3Cr_2Nb_2$	1350	30	1230
Nb(3)	$Al_{93}Fe_3Cr_2Nb_2$	1400	30	1260
Nb–Ti	$Al_{93}Fe_3Cr_2Nb_1Ti_1$	1400	40	1230

This technique allows obtaining high cooling rates but lower than those obtained by melt-spinning.

In the literature there are no previous reports on gas atomization of nano-quasicrystalline Al–Fe–Cr–Nb alloys. However, a few references of gas atomized powders of similar nano-quasicrystalline alloys in the Al–Fe–Cr–Ti system can be found, by Kimura et al. [7], Todd et al. [8], Bartova et al. [9], Vojtech et al. [10] and Yamasaki et al. [11]. None of them however, give details of the melting and atomization processes. Only Todd et al. [8] mention the use of He for atomization, Bartova et al. [9] and Vojtech et al. [10] used N_2 with an atomization pressure of 0.45 and 0.5 MPa respectively, and Yamasaki et al. [11] used high pressure gas atomization using Ar at a dynamic pressure of 9.8 MPa. Considering that Nb has a very high melting point (2469 °C), around 800 °C higher than the melting point for Ti (1670 °C), it is expected that the Al–Fe–Cr–Nb has higher *liquidus* temperature than alloys with Ti instead of Nb. Moreover, the large difference in the melting point of each of the alloy components, particularly in the case of Al and Nb, brings along a big challenge for the melting and for atomization processes in order to obtain the desired spheroidal shapes and a precise powder composition with a homogenous microstructure.

In the present work, the feasibility to produce nano-quasicrystalline Al–Fe–Cr–Nb bars with good mechanical properties by means of gas atomization and consolidation process followed by hot extrusion was investigated.

2. Experimental

Table 1 shows the nominal chemical compositions and the gas atomization main parameters used for producing four alloy powders. Commercial pure Al (99.7 at%), Cr (99.7 at%) and Ti (99.7 at%) elements and a Fe–40Nb (w%) alloy were used to produce ~1 kg of molten alloys. 3 at% of Al was added in excess to the Nb(2), Nb(3) and Nb–Ti alloys in order to compensate for the Al lost because of the evaporation and oxidation on the surface of the melt in the furnace. Thus, the initial alloy compositions were Nb(2) and Nb(3): $Al_{93.203}Fe_{2.913}Cr_{1.942}Nb_{1.942}$ (at%) and Nb–Ti: $Al_{93.203}Fe_{2.913}Cr_{1.942}Nb_{0.971}Ti_{0.971}$ (at%). A graphite crucible was used under an N_2 flow.

After the alloy was melted the crucible was moved to pour the molten alloy in the atomizer. A 6 mm diameter quartz atomizer nozzle was used with an argon atomization pressure of 0.5 MPa. Table 1 shows the thermal conditions used for each atomization run. The runs ended when the melt froze below the *liquidus* temperature in the nozzle. Three atomization runs were done for a nominal composition of $Al_{93}Fe_3Cr_2Nb_2$ (hereafter in at%), and one for $Al_{93}Fe_3Cr_2Nb_1Ti_1$. Ti was added to decrease the *liquidus* temperature and facilitate the melting and atomization process seeking to obtain a more accurate chemical composition with well formed icosahedral quasicrystalline particles.

Atomized powders were sieved in different size ranges between 55 μm and 250 μm. Powders with particle sizes lower than 75 μm of alloys Nb(2) and Nb(3) were cold compacted and extruded at 375 °C with an extrusion ratio of 7.5 and a ram speed of 18 mm/min.

The microstructure of the atomized powders and extruded bars were characterised by X-ray diffraction (XRD) using a Rigaku θ–2θ diffractometer with Cu Kα radiation, Scanning Electron Microscopy (SEM) using a JEOL 6300 with an Oxford Instruments EDX detector, and Transmission Electron Microscopy (TEM) using a Philips CM20. TEM samples from atomized powders were prepared with a final thickness of ~180 nm in a Focus Ion Beam (FIB) FEI 200.

Compression tests at room temperature and at 250 °C of the extruded bars were carried out in an Instron 4204 with a 50kN load cell and a deformation rate of 10^{-3} s^{-1}. Compression samples of 5 mm in diameter and 10 mm in length were polished up to silicon carbide grinding paper P800. Graphite/MoS_2 based grease was applied to both surfaces of the sample for lubrication.

3. Results

All the atomization runs were stopped by the nozzle freeze off impeding the atomization of the whole of the molten alloy. A very small quantity of powder was obtained for the Nb(1) and Nb–Ti alloys. All the atomized powders of the Al–Fe–Cr–Nb alloys had the most abundant weight fraction in the range size of 55–75 μm, however the abundant weight fraction for the Nb–Ti alloy was in the range of 0–55 μm. Table 2 summarises the average chemical compositions of each of the atomized alloys measured by EDX analysis on more than 25 powder particles (for each composition) with particle sizes smaller than 75 μm. It is observed that all atomized powders have Si contamination which is an impurity element in the raw materials used. Nb(1) atomized powder lost a very large quantity of Al, having only 85.5 at% Al. The rest of the alloys have an Al content close to the nominal composition of 93 at% Al. However, it is observed that all the atomized powders have a lower fraction of Nb and Ti than the nominal composition.

As it can be seen in the X-ray diffractograms in Figs. 1 and 2, despite of the discrepancies in the chemical composition respect to the nominal composition, all the atomized powders showed icosahedral quasicrystalline phase (i-phase) for powder size fractions smaller than 75 μm, with the exception of the Nb(1) atomized powder. In Fig. 1 it can be seen the X-ray diffractograms taken for different powder size fractions, from <55 μm up to 250 μm, of the Nb(3) atomized alloy. Fig. 2 shows the X-ray diffractograms taken for all the atomized powders with size fraction from 0 to 75 μm. The presence of the i-phase have also been confirmed by TEM analysis, as can be seen in Fig. 3 trough the fivefold symmetry diffraction pattern taken from the "black" quasi-spherical particle observed in the microstructure of a Nb–Ti atomized powder particle.

The X-ray diffractograms of Nb(1) show the stable phases fcc-Al, Al_3Nb, $Al_{13}Cr_2$ and $Al_{13}Fe_4$ but no peaks of the i-phase were identified for all the powder size fractions (see Fig. 2 for the corresponding diffractogram from the 0 to 75 μm size fraction).

Nb(2) atomized powders which had the higher Al content ~94 at%, also showed the presence of the same four stable crystalline phases mentioned above in all size fractions, but in addition a minor fraction of the i-phase can be clearly identified in the diffractograms up to the powder size of 75 μm (see Fig. 2).

The diffractograms of the Nb(3) atomized powders show the presence of fcc-Al, Al_3Nb and $Al_{13}Cr_2$ phases for all size fractions (see Fig. 1). The icosahedral quasicrystalline phase is clearly observed with peaks at 2θ values: 22.3°, 41.3°, 43.5°, 62.5° and 72.7° for powder sizes up to 75 μm. For larger powder sizes only the two main peaks of the i-phase (at 41.3°, 43.5°) could be indexed. Also some peaks of the intermetallic $Al_{13}Fe_4$ can be observed for each powder size fraction. The complex monoclinic $Al_{13}Fe_4$ phase is easily distorted during the rapid solidification

Table 2
Average chemical composition measured on the atomized powders by EDX analysis.

Alloys	Average measured chemical composition (at%)					
	Al	Fe	Cr	Nb	Ti	Si
Nb(1)	85.5	10.1	1.9	2.2	–	0.3
Nb(2)	94	2	2.45	0.75	–	0.8
Nb(3)	92.8	3.5	2.5	0.8	–	0.4
Nb–Ti	92.5	4.2	2.1	0.5	0.6	0.1

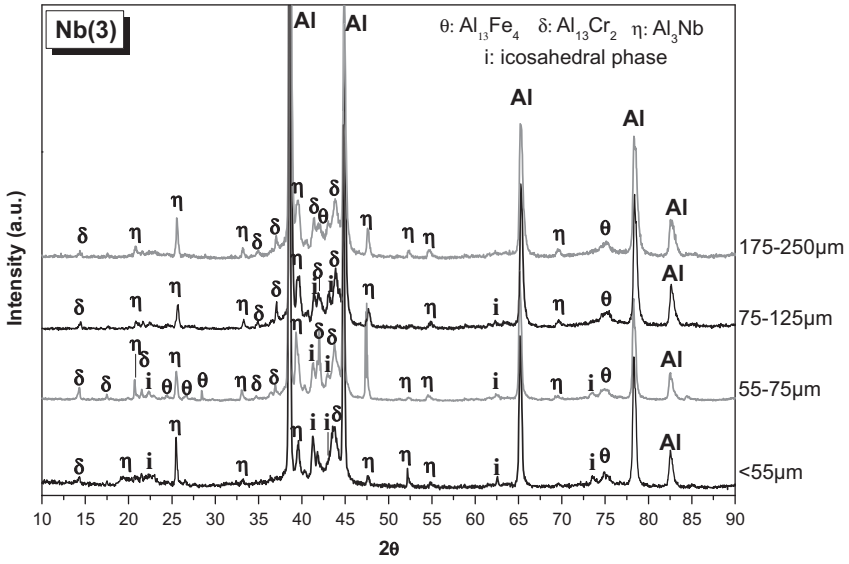

Fig. 1. X-ray diffractograms of the Nb(3) alloy powder for different powder sizes.

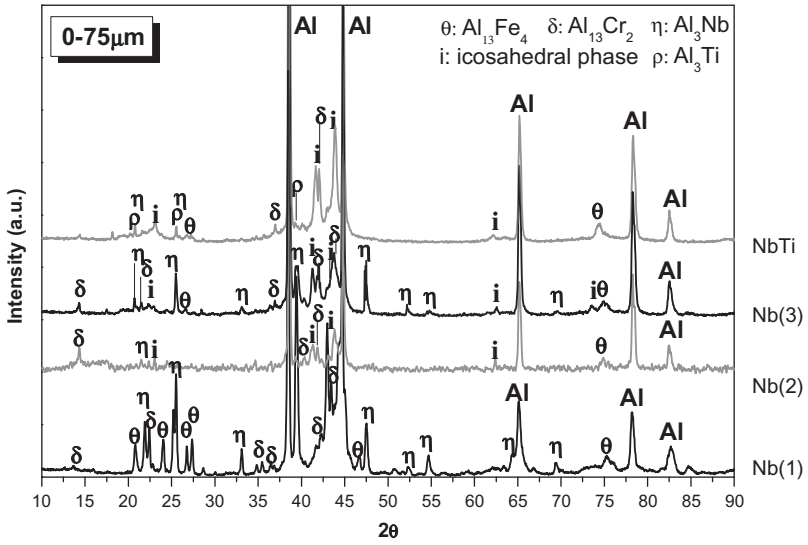

Fig. 2. X-ray diffractograms of 0–75 μm powder size range for all the atomized powder alloys.

process and consequently the diffraction peaks might not be clearly identifiable [12].

The Nb–Ti atomized powders show very similar phases than the Nb(3) powders for all the size fractions, with the exception of the presence of a minor fraction of Al_3Ti (Fig. 2).

Atomized powders were obtained with rounded shape morphology (see Fig. 3a–e), with the exception of the largest sieved powder sizes, typically over 175 μm which showed irregular nodular shapes. Some small satellite particles have been found attached to powder particle of different size fractions (see Fig. 3b and e). The largest powder size particles, particularly over 175 μm showed large Al_3Nb dendrites in the microstructure. However, some Al_3Nb dendrites were found in few powder particles smaller than 175 μm but larger than 75 μm (see Fig. 3d).

Nb(1) powders showed a microstructure formed by many faceted intermetallic compounds. In the powder size smaller than 25 μm the intermetallics are quasi-spheroidal like dendrites up to 2 μm in size. In larger powder sizes, intermetallics had plaques shape up to ~10 μm (see Fig. 3a and b). Nb(2), Nb(3) and Nb–Ti powder samples showed a nanoquasicrystalline microstructure composed by spheroidal icosahedral quasicrystalline particles, and some intermetallic particles embedded in an Al matrix (Figs. 3c–f). The average i-phase particles size increased from ~200 nm up to ~1 μm with the powder size. Also, the intermetallic volume fraction in the microstructure increased as the i-phase volume fraction decreased with powder size as it was observed in the X-ray diffractograms (see Fig. 1).

Two solid bars were obtained by cold compaction followed by hot extrusion from Nb(2) and Nb(3) atomized powders with powder particle sizes lower than 75 μm. The powder size was selected in order to produce a solid bar with nanoquasicrystalline microstructure. Nb(1) was not used for extrusion because had a chemical composition far from the target composition of 93 at% Al. It was not possible to extrude Nb–Ti powder due to the low quantity of powder obtained.

Fig. 4 shows the X-ray diffractograms of powder samples made from both extruded bars from Nb(2) and Nb(3) atomized powders. Both samples had the same phases: fcc-Al, i-phase, Al_3Nb, $Al_{13}Cr_2$

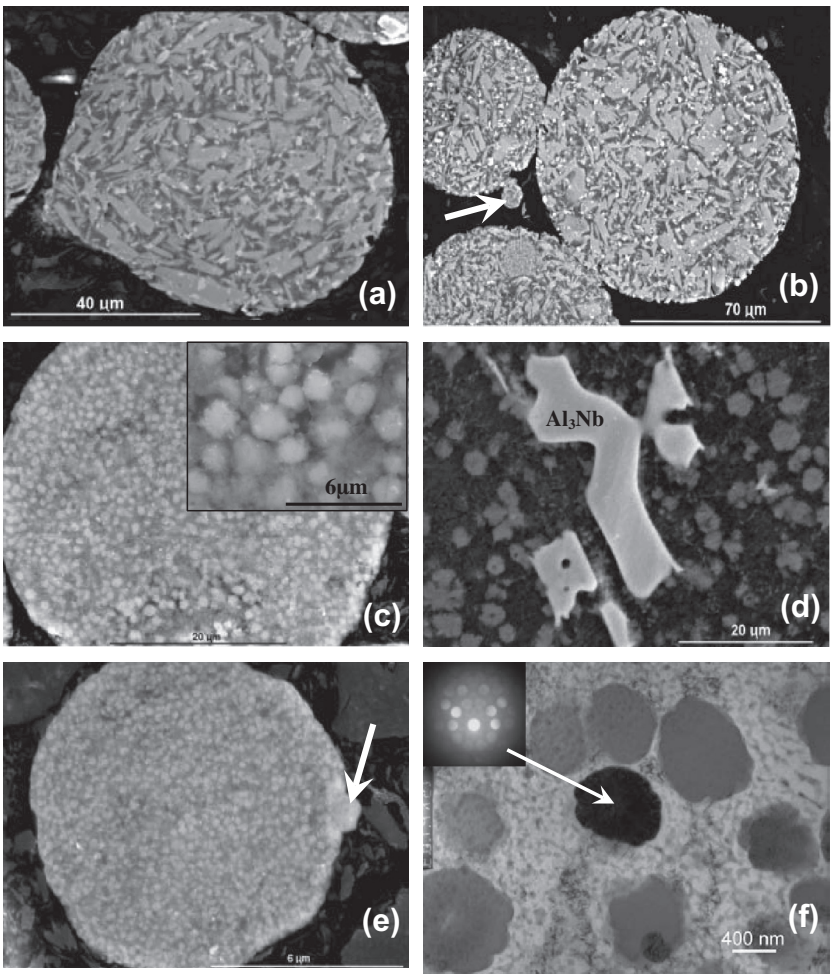

Fig. 3. Microstructure of atomized powders. Secondary electron images of: (a) Nb(1) < 55 µm; (b) Nb(1) 55–75 µm, arrow indicated a satellite particle. (c) Nb(3) < 55 µm, inset shows the microstructure at higher magnification; (d) Nb(3) 75–125 µm; (e) Nb–Ti < 55 µm, arrow indicated a satellite particle. TEM bright field images of: (f) Nb–Ti 55–75 µm, inset: fivefold symmetry conversion beam electron diffraction pattern from the icosahedral particle marked with an arrow.

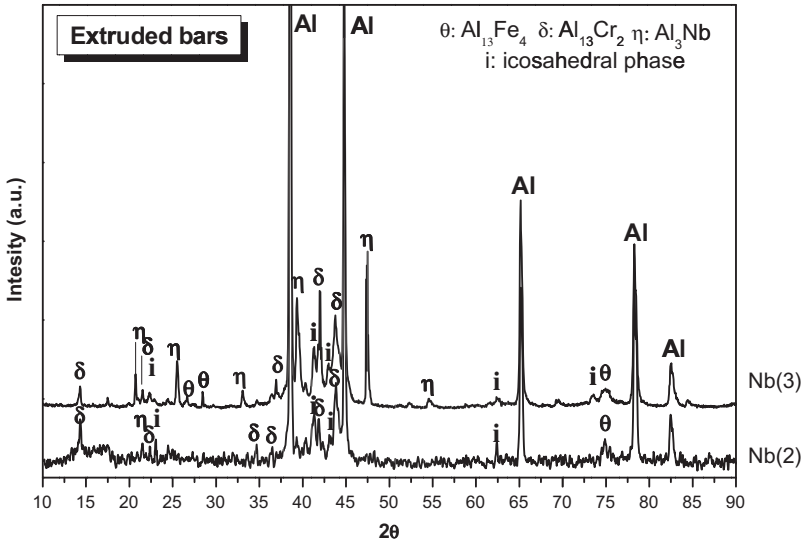

Fig. 4. X-ray diffractograms of Nb(2) and Nb(3) extruded bars.

and $Al_{13}Fe_4$ that were present in the atomized powders used for extrusion. Moreover, Fig. 5 shows that the nanoquasicrystalline microstructure from the atomized powders was preserved in the extruded bars. No cracks and few porous were observed.

Fig. 6 shows the engineering stress–strain compression curves for both bars, Nb(2) and Nb(3), tested at room temperature and at 250 °C. The compression curves of the Nb(2) as well as the corresponding to Nb(3) show similar features, such as the same elastic

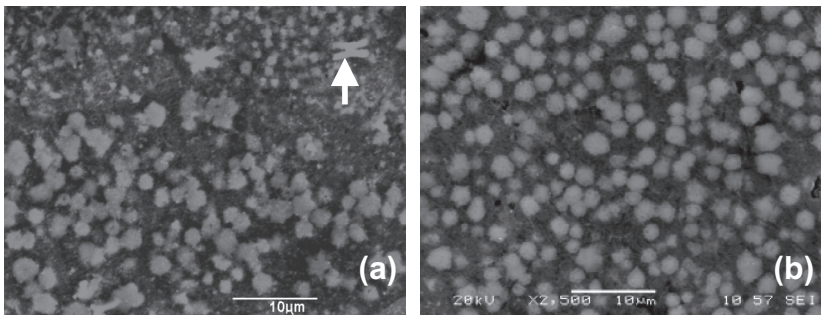

Fig. 5. Secondary electron image of the microstructure of the extruded bars from powder size under 75 μm of: (a) Nb(2) and (b) Nb(3). Arrow indicates an Al_3Nb particle.

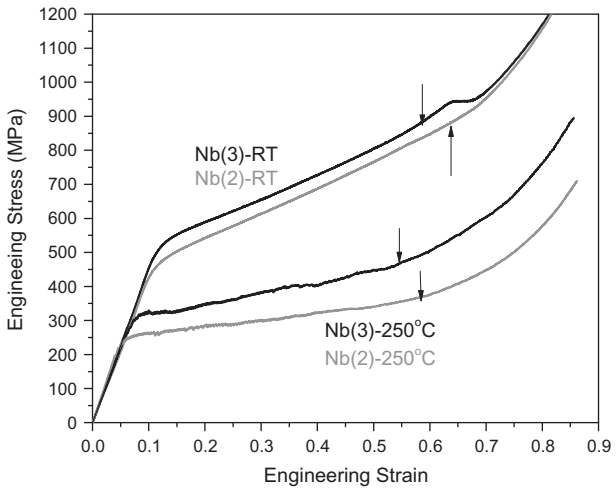

Fig. 6. Engineering stress–strain compression curves at room temperature (RT) and at 250 °C from the bars extruded from the Nb(2) and Nb(3) alloy powders. Arrows indicate the point at slope change which would be related with an inhomogeneous deformation due to the barreling effect.

and plastic slopes. However, as it was expected, the extruded bar from Nb(3) powder, which had lower Al content (92.8 at%), developed higher yield stress values than the Nb(2), which had 94 at% Al. Barreling effect was observed to occur earlier at 250 °C than at room temperature, but for all the cases this happened after 50% of strain.

4. Discussion

4.1. Melting and atomization

The melting temperature and the long holding time used for preparing the Nb(1) alloy was not enough to dissolve the Cr in the melt, though the Al evaporation was considerable and the chemical composition of the atomized powder was far from the alloy target composition. The decrease in the Al content produced an increase in the *liquidus* temperature that reduced the temperature range for atomization; the freezing of the nozzle happened soon after the start of the atomization thus yielding little quantity of powder. In order to obtain a longer atomization run for an Al alloy with 85.5% Al (like Nb(1)) the starting atomization temperature should be higher than 1250 °C.

Considering the results of the atomization run for the Nb(1) batch, an extra of 3% Al content was added in the second batch (Nb(2)) in order to compensate the Al evaporation fixing the holding time in 30 min at a melting temperature of 1350 °C, which would also help for dissolving the Cr in the melt. These melting conditions would maintain the melt composition close to the target composition therefore it was considered to start the atomization at 1230 °C. The results (Table 2) showed the melting temperature was sufficient for dissolving the Cr, but higher temperature or a longer time would be necessary for dissolving the Fe–40Nb master alloy completely. The selected starting atomization temperature allowed obtaining a larger quantity of the atomized powder.

For the Nb(3) batch, in order to improve the dissolution of Cr and of the Fe–40Nb master alloy the melting temperature was increased up to 1400 °C (see Table 1). The atomization started at 1260 °C and larger fraction (~60%) of the molten alloy was atomized. This was the best combination of melting and atomization parameters obtained for the $Al_{93}Fe_3Cr_2Nb_2$ alloy. However, the Nb content in the atomized powder remained lower than the target composition (see Table 2).

In order to reduce the *liquidus* temperature and improve the dissolution of Nb, half of the Nb content in the nominal composition was substituted by Ti. Thus, the Nb–Ti batch was processed at the same melting temperature but with a longer holding time of 40 min. The atomization temperature was reduced to 1230 °C. An improvement in the melting process was obtained increasing the dissolution of Nb and Ti, and resulted in the highest content of Nb + Ti in the powder composition among all the atomized batches (see Table 2). However, the atomization process was not highly successful. The starting atomization temperature selected produced good spheroidal shape powder with very fine sizes (<55 μm), but the larger powder size contained Al_3Nb dendrites that solidified in the liquid before reaching the atomization zone. The powder quantity was small because the nozzle freezed off within a short time due to the temperature difference between *liquidus* and *solidus* for this alloy being smaller than that for the Al–Fe–Cr–Nb alloys.

It is observed for the alloys studied, that a heater in the conducting tube towards the nozzle would be necessary in order to obtain a stable atomization run at a constant temperature allowing the production of very uniform powders with a narrow size distribution and a high yield ratio (atomized mass/molten mass).

4.2. Powder microstructure

The larger powder size fractions, typically over 175 μm, showed no i-phase and large Al_3Nb dendrites which would grow before the melt reached the atomization zone. With the exception of the Nb(1) batch that was obtained with chemical composition far from the target composition of $Al_{93}Fe_3Cr_2Nb_2$, the rest of batches have shown a microstructure composed by i-phase and stable intermetallics compounds embedded in an fcc-Al matrix for powder particles smaller than 75 μm (Figs. 1 and 2). Similar results were obtained by Todd et al. [8] who found the i-phase up to 100 μm powder sizes for an $Al_{93}Fe_3Cr_2Ti_2$ atomized alloy.

Nb(2), with lower Fe than Cr content, showed a lower fraction of the $Al_{13}Fe_4$ than the Nb(3) and Nb–Ti powders which had a ratio of Fe/Cr >1 (see Table 2). Similar gas atomized alloys in the Al–Fe–Cr–Ti system showed similar microstructure features though with different stable intermetallic compounds [7–11]. Vojtech et al. [10] observed for an $Al_{95}Cr_{3.1}Fe_{1.1}Ti_{0.8}$ alloy a microstructure composed by i-phase and the stable phases $Al_{13}Cr_2$ and $Al_{13}Fe_4$ embedded in an fcc-Al matrix. Kimura et al. [7], Todd et al. [8] and Yamasaki et al. [11] reported only the presence of i-phase and $Al_{23}Ti_9$ (or Al_3Ti in ref [11]) embedded in the fcc-Al matrix. Neither in those works nor in the present work the presence of the metastable θ-$Al_{13}(Fe,Cr)_{2-4}$ phases was observed, which was found in the Al–Fe–Cr–Ti/Nb melt-spun samples [3–5]. Although the melt-spinning technique can reach higher cooling rates than the gas atomization technique, both techniques can lead to obtaining similar microstructures in the Al–Fe–Cr based alloys. Nonetheless, different processing conditions and atomizers' configuration can produce atomized powders with different metastability having different stable and metastable intermetallics embedded in the fcc-Al matrix for the same alloy composition. For example, He atomizing gas produces smaller droplets than N_2, which is attributed to higher gas velocity [13]. High Pressure Gas Atomizers (HPGA) uses a pulverizing effect of shock waves of an under-expanded gas flow promoting a higher quenching rate [14]. These different processing conditions can explain the different intermetallic compounds obtained for the Al–Fe–Cr–Ti atomized powders by the different authors [7–11].

4.3. Extruded bars

The atomized powder under 75 μm size from batches Nb(2) and Nb(3) were extruded at 375 °C. Fig. 4a and b shows the X-ray diffractograms of powder samples taken from the extruded bars Nb(2) and Nb(3) respectively. The diffractograms show that the extrusion process did not affect the phase distribution in the bars' microstructure respect to the atomized powder used for producing these bars (Figs. 1 and 2). This result is in agreement with the calorimetry results and phase transformation studies carried out in previous works on melt-spun samples of the $Al_{93}Fe_3Cr_2Nb_2$ alloy [4–6]. No microstructural changes were observed for the melt-spun samples after heat treatment at 400 °C for 66 h and no phase distribution changes were observed after heat treatment for 30 min at 450 °C. Those results suggest that the Al–Fe–Cr–Nb alloy atomized powder could be extruded at least up to 450 °C without changes in the phase distribution.

This work reports for the first time extruded bars from Al–Fe–Cr–Nb alloy atomized powders. Fig. 5a and b shows the microstructures of the bars from the Nb(2) and Nb(3) batches respectively. The microstructure of the extruded bar from the Nb(2) batch had certain grade of heterogeneity as different powder sizes were used. Zones with different particles sizes can be seen in the microstructure showed in Fig. 5a. An Al_3Nb particle is also observed indicated by an arrow in the picture and identified by EDX analysis. The extruded bar from the atomized powder of the Nb(3) batch had a more homogeneous microstructure (Fig. 5b) which can be related with the narrow powder size distribution obtained for this batch.

Both bars show a microstructure containing large fraction of spheroidal particles, which in correspondence with the X-ray diffractograms (Fig. 4) could be the i-phase. The particles volume fraction (f) determined by image analysis was ~0.40 and ~0.45 for Nb(2) and Nb(3) respectively, which are in good agreement with the results on melt-spun samples reported by Audebert et al. [3]. The authors found $f \sim 0.42$ and $f \sim 0.46$ for $Al_{93}Fe_3Cr_2Ti_2$ and $Al_{91}Fe_5Cr_2Ti_2$ alloys respectively. The size of the particles found in the present work, was between 800 nm and 1.5 μm, which is in agreement with the particles sizes found in the atomized powders.

Other authors found similar microstructures and smaller i-phase particles sizes in extruded bars of atomized powders of Al–Fe–Cr–Ti alloys [8,10]. Kimura et al. [7] found i-phase particles of 600 nm to 900 nm in an extruded bar of <75 μm powder size fraction of the $Al_{92}Fe_3Cr_3Ti_2$ alloy. Yamasaki et al. [11] found only 8%vol fraction of i-phase particles with size around 250 nm to 500 nm in a bar extruded at 500 °C from atomized powder of $Al_{92.5}Fe_{2.5}Cr_{2.5}Ti_{2.5}$ alloy produced in a high pressure gas atomizer. Finally, considering the few results reported for atomized and extruded bars of Al–Fe–Cr–Ti alloys in the literature and the ones obtained for the Al–Fe–Cr–Nb alloys in the present work, some guidelines can be written as good practice for obtaining extruded bars of the $Al_{93}Fe_3Cr_2Nb_2$ alloy with a very refined microstructure containing a large fraction of i-phase:

(i) The best conditions for obtaining this microstructure in the gas atomization process is using a high pressure gas atomizer and including a heater in the conducting tube for maintaining the molten alloy at ~1250 °C during the atomization.
(ii) The powder size range should be selected having a large i-phase fraction typically smaller than 75 μm. The extrusion temperature should not be higher than 450 °C.

4.4. Mechanical behavior

The compression tests allow investigating the stress–strain response of the material up to large strains, in contrast to the tensile tests where necking produces a localized plastic deformation reducing uniform deformation in the testing sample. However, due to the high compressive force applied between the anvils and the testing sample, friction can affect the stress–strain response of the material tested with a non homogeneous strain flow. The major side-effect of friction is the occurrence of barreling (cylindrical sample become in a barrel shape). Moreover, during hot forging manufacture, the barreling effect is more pronounced because of the heat transfer between the hot metal and the cooler die. The metal nearer to the die surfaces will cool faster than the metal towards the center of the part. The cooler material is more resistant to deformation and will expand less than the hotter material in the center, also causing a barreling effect. During the compression tests done in the present work, as the samples were very small in comparison with the load train which was inside of the furnace chamber, no gradient along the sample and compression platens was observed. Therefore, the barrel shape observed in the tested samples was only due to the friction forces which increased with the compression load. Lovato and Stout [15] studied the effect of friction (including the effect of the lubricant) on the stress–strain response during compressive tests. They showed that no significant influence of the lubrication was observed for strains lower than 0.5.

In Fig. 6, arrows indicated the possible points where the barreling effect could have started for each compression test. It is observed that for all the tests the significant change in the stress related to the barreling effect appear between strain values of 0.5 and 0.6. It is also observed that the lubricant used was less effective at 250 °C, which induces a barreling effect at lower strain values than at room temperature. Finally, in accordance with Lovato and Stout [15], only strain levels up to 0.5 could be assumed as homogeneous deformation.

When comparing the compression curves at room temperature with the ones at 250 °C, it can be seen that the strain hardening coefficient ($d\sigma/d\varepsilon$) decreases with the temperature. On other hand, when contrasting the Nb(2) with the Nb(3) alloy tested at the different temperatures it is observed that the larger particle volume

fraction that Nb(3) has respect to Nb(2) provides additional strengthening by the Orowan mechanism increasing the yield compressive stress ($\sigma_{0.2\%}$) from 450 MPa for Nb(2) to 500 MPa for Nb(3) at room temperature and from 250 MPa for Nb(2) to 300 MPa for Nb(3) at 250 °C. However, there is not a clear difference in strain hardening behaviour between the two alloys.

Luo et al. [16], reported a tensile/compression asymmetry in an intermediate range of temperatures for the nanoquasicrystalline $Al_{93}Fe_3Cr_2Ti_2$ alloy extruded from mechanical alloyed powders. Considering the brittle behavior that their tensile curves showed it is not certainly clear that those results show the asymmetry claimed. However, it is reasonable to think that the alloy has that kind of asymmetry. The stress required for homogeneous dislocation nucleation is highly dependent on the crystallographic orientation and the uniaxial loading conditions; certain orientations require a higher stress in compression than in tensile loading [17]. Thus, for a multi grain isotropic pure metallic phase material the macroscopic behavior cannot show any asymmetry between tensile and compression tests [18]. However, plastic deformation processes, as extrusion, can produce a crystallographic texture in the materials microstructure that can induce tensile/compression asymmetry. Moreover, bimodal grain size or partial re-crystallized alloys microstructures can show a tensile/compression asymmetric behavior [19]. This asymmetry has been reported as a fundamental property of nanocrystalline materials by Hayes et al. [20] and Cheng et al. [21]. In the later reference, the authors developed a model that explain the different deformation mechanisms involved for the different grain size ranges, in which they predict an important change in the dislocation sources from nano-size grains to coarse grains sizes in the range of 500–1000 nm. Al grain sizes under 1000 nm are normally observed for rapid solidified Al-based alloys [3,5]. Thus, it is reasonable that the extruded Al–Fe–Cr–Nb alloys in the present work have Al grains under 1000 nm and have a tensile/compression asymmetry. Therefore, the compressive yield stress values obtained for Nb(2) and Nb(3) alloys should be compared with the yield stress values determined for other alloys in compression tests. Vojtech et al. [10] found a compressive yield stress (Ycs) at room temperature of 465 MPa for an $Al_{95}Cr_{3.1}Fe_{1.1}Ti_{0.8}$ (at%) alloy extruded at 480 °C from atomized powders, and Luo et al. [16] for an $Al_{93}Fe_3Cr_2Ti_2$ (at%) alloy extruded at 500 °C from mechanical alloyed powders obtained 560 MPa and 260 MPa of Ycs at room temperature and at 300 °C respectively. No Ycs value was found in the literature for an Al–Fe–Cr–Nb alloy. To the best of the author's knowledge this is the first report on bulk production of alloys in this system. Considering the difference in the chemical composition and processing routes, the Ycs obtained in the present work are in the same range of the Ycs values found for similar bulk Al–Fe–Cr–Ti alloys [10,16]. Moreover, it worth mentioning that the alloys studied, from the Al–Fe–Cr–Nb systems, show a very strong ability to retain the strength at elevated temperature, as expected and was predicted by previous works done on melt-spun ribbons [4–6]. Moreover, it is observed that up to 250 °C the strength (Ycs) is reduced only up to 60% of the strength at room temperature, in contrast to the commercial Al alloys for which normally the strength fell down to 10–30% [22].

5. Conclusions

Gas atomized nanoquasicrystalline Al–Fe–Cr–Nb powders and extruded bars were obtained, and the microstructure and the mechanical properties of the bars were characterized for the first time to best of the author's knowledge.

Four gas atomization runs of alloys from the Al–Fe–Cr–(Nb,Ti) system varying different processing parameters such as the *maximum melt holding temperature, melting and holding time, and initial melt temperature in the atomization nozzle* were done. Guide lines were given as good practice for achieving a high efficient atomization run of the new nanoquasicrystalline $Al_{93}Fe_3Cr_2Nb_2$ (at%) alloy:

- For achieving the correct chemical composition of $Al_{93}Fe_3Cr_2Nb_2$ (at%), due to the high melting point components (Cr, Ti and Nb) a high melt temperature (1450 °C during 30 min) is required and around 3% of extra Al fraction is needed to compensate the loss of Al by evaporation.
- Changes in the chemical composition of the $Al_{93}Fe_3Cr_2Nb_2$ (at%) alloy can drastically affect the ability to form icosahedral quasicrystalline particles.
- A large fraction of the icosahedral quasicrystalline particles is only found for powder size fractions typically lower than 75 μm.
- In order to obtain high quality atomized powders (spherical powder with a refined microstructure), the pre-atomization growth of Al_3Nb intermetallic dendrites should be avoided and preventing an early nozzle freezing is recommended to keep the melt atomization temperature constant using a heater in the melt conduct to the atomization nozzle.
- The atomization melt temperature should be around 1250 °C in order to obtain spherical powders with a refined microstructure containing large fraction of icosahedral quasicrystalline particles.
- Higher atomization melt temperature than 1250 °C can produce large fraction of small satellite powder particles, which will deteriorate the mechanical properties of the extruded bars.
- Si contamination up to 0.8 at% can be tolerated as it has not had an important effect on the microstructure of the nanoquasicrystalline $Al_{93}Fe_3Cr_2Nb_2$ (at%) alloy.

A good microstructure, consisting of a very refined nanoquasicrystalline particles embedded in an fcc-Al matrix, in extruded bars can be obtained (1) using powder size ranges lower than 75 μm, (2) avoiding the formation of satellite powder particles and (3) using an extrusion temperature not higher than 450 °C.

The mechanical properties of nanoquasicrystalline alloys close to the nominal composition of $Al_{93}Fe_3Cr_2Nb_2$ (at%) at room temperature have strength values similar to the highest strength values obtained for commercial Al alloys. However, as it was predicted the strength at elevated temperature (250 °C) remains extremely high (60% of the one at room temperature) in comparison to commercial Al alloys. Moreover, the specific strength at elevated temperature of these alloys is highly competitive with Ti alloys, which can open a new market for these alloys by the substitution of the more expensive Ti alloys by these lighter and cheaper Al based nanoquasicrystalline alloys.

Acknowledgements

This work was financially supported by UBACyT 2010/058, PICT-Oxford 2010/2831 and the cooperation SECyT-CAPES project. Dr. M. Galano thanks the RAEng for their support in research.

References

[1] H. Jones, Mat. Sci. Eng. A304-306 (2001) 11–19.
[2] A. Inoue, Prog. Mater. Sci. 43 (1998) 365–520.
[3] F. Audebert, F. Prima, M. Galano, M. Tomut, P. Warren, I.C. Stone, B. Cantor, Mater. Trans. JIM 43 (2002) 2017–2025.
[4] M. Galano, F. Audebert, B. Cantor, I.C. Stone, Mater. Sci. Eng. A 375–377 (2004) 1206–1211.
[5] M. Galano, F. Audebert, I.C. Stone, B. Cantor, Acta Mater. 57 (2009) 5107–5119.
[6] M. Galano, F. Audebert, I.C. Stone, B. Cantor, Philos. Mag. Letter 88 (2008) 269–278.
[7] H. Kimura, A. Inoue, K. Sasamori, J. Mater. Trans. JIM 41 (2000) 1550–1554.

[8] I. Todd, Z. Chlup, J. O'Dwyer, M. Lieblich, A. García-Escorial, Mater. Sci. Eng. A 375–377 (2004) 1235–1238.
[9] B. Bartova, D. Vojtech, J. Verner, A. Gemperle, V. Studnicka, J. Alloys Comp. 387 (2005) 193–200.
[10] D. Vojtech, A. Michalcova, F. Prusa, K. Dam, P. Seda, Mater. Charact. 66 (2012) 83–92.
[11] M. Yamasaki, Y. Nagaishi, Y. Kawamura, Scripta Mater. 56 (2007) 785–788.
[12] F. Audebert, in: B. Idzikowski, P. Švec, M. Miglierini (Eds.), Properties and Applications of Nano-Crystalline Alloys from Amorphous Precursors, Nato Science Series II: Mathematics, Physics and Chemistry, vol. 184, Kluwer Acad. Publishers, Dordrecht, 2005, pp. 301–312.
[13] A. Unal, Mater. Sci. Technol. 4 (1988) 909–915.
[14] I.E. Anderson, R.S. Figliola, H. Morton, Mater. Sci. Eng. A 148 (1991) 101–114.
[15] M.L. Lovato, M.G. Stout, Met. Mater. Trans. A 23 (1992) 935–951.
[16] H. Luo, L. Shaw, L.C. Zhang, D. Miracle, Mater. Sci. Eng. A 409 (2005) 249–256.
[17] M.A. Tschopp, D.L. McDowell, Appl. Phys. Lett. 90 (2013). 121916–121916(3).
[18] B.Q. Han, Z. Lee, S.R. Nutt, E.J. Lavernia, F.A. Mohamed, Metall. Mater. Trans. A 34 (2003) 603–613.
[19] B.Q. Han, E.J. Lavernia, F.A. Mohamed, Mater. Sci. Eng. A 358 (2003) 318–323.
[20] R.W. Hayes, R. Rodriguez, E.J. Lavernia, Acta Mater. 49 (2001) 4055–4068.
[21] S. Cheng, J.A. Spencer, W.W. Milligan, Acta Mater. 51 (2003) 4505–4818.
[22] Heat Treater's Guide: Practices and Procedures for Nonferrous Alloys, Ed. Harry Chandler, ASM International, USA. 1996.